Nano Res. 2012, 5(8): 531–542
DOI 10.1007/s12274-012-0238-x
Research Article

ISSN 1998-0124
CN 11-5974/O4

Ultrasmall Fluorescent Silver Nanoclusters: Protein Adsorption and Its Effects on Cellular Responses

Li Shang[1], René M. Dörlich[1], Vanessa Trouillet[2], Michael Bruns[2], and G. Ulrich Nienhaus[1,3] (✉)

[1] Institute of Applied Physics and Center for Functional Nanostructures (CFN), Karlsruhe Institute of Technology (KIT), Wolfgang-Gaede-Strasse 1, 76131 Karlsruhe, Germany
[2] Institute of Materials Research III, Karlsruhe Institute of Technology (KIT), Hermann-von-Helmholtz-Platz 1, 76344 Karlsruhe, Germany
[3] Department of Physics, University of Illinois at Urbana-Champaign, Urbana, Illinois 61801, USA

Received: 21 March 2012 / Revised: 27 April 2012 / Accepted: 8 June 2012

ABSTRACT

Ultrasmall silver nanoclusters (AgNCs) are a novel type of fluorescent nanoprobes that have aroused a great deal of interest in recent years. In view of many promising applications in biological research, it is of great importance to explore their behavior in the complex biological environment. In this study, interactions of AgNCs with a model protein, human serum albumin (HSA), have been systematically investigated by using a variety of techniques including absorption spectroscopy, steady-state and time-resolved fluorescence, as well as circular dichroism spectroscopy. The results show that the physicochemical properties of both proteins and AgNCs undergo changes upon their interactions; however, it appears that the overall conformation of HSA remains essentially unaffected in the complex. Binding of HSA to AgNCs was assessed by measuring tryptophan fluorescence quenching of HSA by AgNCs. Furthermore, biological implications of protein adsorption were quantitatively explored by evaluating responses of HeLa cells to AgNC exposure through live-cell fluorescence microscopy and a cytotoxicity test, revealing that protein adsorption has a significant effect on the biological response to AgNC exposure.

KEYWORDS

Silver nanoclusters, protein adsorption, cytotoxicity, cellular uptake, fluorescent probes

1. Introduction

With the rapid development of nanoscience and nanotechnology, a wide variety of nanomaterials have been synthesized and found promising applications in biology and biomedical research [1–3]. Metal nanoclusters (NCs), composed of a few to roughly a hundred atoms, have emerged as a novel type of nanomaterials that have received much attention in recent years [4]. These NCs provide the bridge between atomic and nanoparticle behavior in noble metals and have, consequently, attracted a great deal of attention. With sizes comparable to the Fermi wavelength of electrons, metal NCs possess properties very distinct from larger metal nanoparticles. Most importantly, these NCs can exhibit strong photoluminescence [5]. For instance, a fluorescence quantum yield (QY) as high as 64% has been reported for silver nanoclusters

Address correspondence to uli.nienhaus@kit.edu

(AgNCs) prepared in organic scaffolds (e.g., DNA) [6]. Besides high brightness, AgNCs possess other attractive photophysical properties including large Stokes shifts and two-photon absorption cross sections [7]. The emission wavelength of AgNCs can be easily tuned from the blue to near-infrared region by varying the type of capping ligands or controlling their core sizes [8, 9]. Moreover, the overall size of fluorescent AgNCs is extremely small in comparison to other luminescent nanomaterials such as semiconductor quantum dots and rare earth up-converting nanoparticles, making them attractive as fluorescent biomarkers because the investigated biological processes are likely minimally perturbed by AgNC-based labeling [10]. Therefore, fluorescent AgNCs hold great potential as novel optical probes and may find wide application in biological research [11–13].

Indeed, recent studies have demonstrated the usefulness of fluorescent AgNCs in biodetection and biological imaging. For example, by virtue of the highly sequence-dependent generation of fluorescent AgNCs in hybridized DNA duplex scaffolds, Guo et al. [14] developed a AgNC-based fluorescence assay capable of identifying the sickle cell anemia mutation in the hemoglobin beta chain gene. Dickson and coworkers [15] showed that fluorescent AgNCs encapsulated by intracellular peptides could be utilized to stain NIH 3T3 cells; they observed that these ultrasmall NCs were incorporated and distributed evenly within cells. Recently, Yin et al. [16] reported that fluorescent AgNC–aptamer assemblies, synthesized via a convenient one-step process, enabled specific recognition and labeling of target tumor cells by fluorescence imaging. While many investigations focus primarily on a particular biological application of fluorescent AgNCs, the general knowledge of their behavior in the complex biological environment is still rather limited. As a matter of fact, it is well known that the surfaces of nanomaterials are immediately covered by biomolecules (e.g., proteins) upon exposure to a biological medium, which may affect the subsequent biological responses [17–21]. Ultrasmall AgNCs have an extremely high surface-to-volume ratio, and we expect significant interactions between proteins and NCs. Moreover, the immediate environment has a strong effect on the fluorescent properties of metal NCs, and pronounced optical changes have been reported upon protein adsorption in biological medium [22]. Correspondingly, in order to further advance the development of AgNC-based functional and safe materials, it is essential to achieve a comprehensive understanding of the NC-protein interactions and their possible biological implications [23, 24].

Thus, here we present a detailed study on the interactions between fluorescent AgNCs and proteins. While previous studies reported fluorescent metal NCs coated with serum proteins during synthesis [25, 26], our current work rather focuses on the interactions of proteins in their native state with pre-formed, small ligand-protected AgNCs. Human serum albumin (HSA) was chosen as a model protein owing to its abundance in the human blood plasma and well-characterized properties [19]. A variety of techniques including absorption spectroscopy, steady-state and time-resolved fluorescence as well as circular dichroism spectroscopy were employed to characterize changes in the properties of AgNCs and proteins upon their interaction. Furthermore, possible biological implications of protein adsorption were quantitatively explored by analyzing cellular responses toward AgNCs by means of fluorescence microscopy and a cytotoxicity test.

2. Materials and methods

2.1 Reagents

Lipoic acid, silver nitrate ($AgNO_3$), HSA (lyophilized powder, essentially fatty acid free, $\geqslant$96%) and thiazolyl blue tetrazolium bromide (MTT) were purchased from Sigma-Aldrich (St. Louis, Missouri, USA). Sodium borohydride ($NaBH_4$) and dimethylsulfoxide (DMSO) were obtained from Carl Roth (Karlsruhe, Germany). Sulforhodamine 101 (1 mmol/L in ethanol), Dulbecco's modified Eagle's medium (DMEM) and CellMask™ DeepRed plasma membrane stain solution (5 mg/mL in DMSO) were purchased from Invitrogen (Leiden, The Netherlands). For all aqueous solutions, high-purity deionized water from a Millipore system was used.

2.2 Synthesis of dihydrolipoic acid-capped AgNCs (DHLA–AgNCs)

DHLA–AgNCs were synthesized by a strategy that was modified from a previous report [27]. Typically, 60.8 mg of lipoic acid were solubilized in 15 mL of an aqueous solution containing 0.18 mL of sodium hydroxide solution (2 mol/L), followed by addition of 0.10 mL of $AgNO_3$ aqueous solution (0.2 mol/L). After stirring for 5 min, 0.80 mL of freshly prepared $NaBH_4$ aqueous solution (0.12 mol/L) was added slowly to the mixture under rapid stirring. The reaction was stopped after stirring for 2 h, and the solution was stored at 4 ℃ in the dark until used. AgNCs were purified by centrifugation filtration, using Nanosep filters (Pall Nanosep, Ann Arbor, MI) with a molecular weight cut-off of 10 kDa. The reddish AgNCs remaining on the filter were re-suspended in phosphate-buffered saline (PBS, containing monobasic potassium phosphate, sodium chloride and dibasic sodium phosphate, pH 7.4, Invitrogen) for the experiments.

2.3 Characterization of DHLA–AgNCs

UV–Vis absorption spectra were recorded with a Cary 100 spectrophotometer (Varian, Palo Alto, USA); fluorescence spectra were taken on a Fluorolog-3 Spectrofluorometer (HORIBA Jobin Yvon, Edison, USA). X-ray photoelectron spectroscopy (XPS) measurements were carried out on a K-Alpha XPS spectrometer (ThermoFisher, E. Grinstead, UK), using Al Kα X-ray radiation (1486.6 eV) for excitation. All spectra were referenced to the C1s peak at 285.0 eV. Dynamic light scattering (DLS) and zeta potential experiments were performed by using a Zetasizer Nano-ZS (Malvern Instruments, Malvern, UK) with a 633 nm laser at 20 ℃.

Atomic force microscopy (AFM) images were measured with a NanoWizard Ⅱ AFM (JPK Instruments, Berlin, Germany) mounted on top of an AxioObserver A1 inverted microscope (Carl Zeiss, Jena, Germany). Samples for AFM measurement were prepared as follows [28]. A piece of freshly cleaved mica was incubated for 5 min with 10 μL of cysteamine solution (10 mmol/L), which had been filtered over a 0.02 μm membrane filter (Whatman, Maidstone, England). Afterwards, the mica was washed with deionized water and dried under a gentle nitrogen flow. Then 10 μL of an aqueous solution containing DHLA–AgNCs (50 μg/mL) was dropped on the mica surface and left to adsorb for 5 min. After washing with deionized water, the mica was dried under a gentle nitrogen flow and used for AFM imaging.

Fluorescence lifetimes were measured with a Microtime 200 confocal microscopy system (PicoQuant, Berlin, Germany) equipped with a water immersion objective (1.2 NA, 60×) (Olympus, Tokyo, Japan) and a pulsed diode laser (LDH-D-C-405, 404 nm, PicoQuant) with 666 kHz repetition rate. The picosecond-laser-excited fluorescence, after passing through a band-pass filter 617/73 (Semrock, Rochester, NY), was collected and detected by a photon avalanche diode (Microphoton Devices, Bolzano, Italy).

2.4 Interaction of DHLA–AgNCs with HSA

The stock solution of HSA was prepared in PBS and purified using micro Bio-Spin chromatography columns (Bio-Rad, Hercules, USA). The molar concentration of HSA was measured spectrophotometrically using an extinction coefficient of 37 000 L/(mol·cm) at 278 nm. The particle concentration of the AgNCs was calculated based on the assumption that all Ag in $AgNO_3$ was reduced to form AgNCs, each consisting of five Ag atoms [27]. To retain the proteins in their native states in the solution as well as to prevent possible disruption to the structure of the AgNC–protein complex, separation techniques (i.e., centrifugation or filtration) to remove free proteins from the solution were entirely avoided. In order to minimize self-absorption and inner filter effects in the fluorescence measurements, dilute solutions of both HSA and AgNCs were used so as to ensure that the absorbance at the excitation wavelength was always less than 0.05. Circular dichroism (CD) measurements were performed on a J-815 CD spectrometer (JASCO Deutschland, Gross-Umstadt, Germany) with a 0.1 cm path length standard cell at 20 ℃. CD spectra were taken in the wavelength range 195–350 nm; each spectrum was an average over six scans. Also, both fluorescence and CD spectra were corrected for buffer solution background.

2.5 Cytotoxicity assays

HeLa cells were cultured as described previously [29].

For the MTT cytotoxicity assay of DHLA–AgNCs, cells were seeded in a 24-well plate (ca. 4×10^4 cells/well) in cell medium over night and, subsequently, incubated with different concentrations of AgNCs (0, 25, 75 and 150 μg/mL) in cell medium for 2 h at 37 ˚C and 5% CO_2. After removing AgNC-containing medium and washing three times with PBS, cells were further incubated in cell medium for 24 h at 37 ˚C and 5% CO_2. Afterwards, cells were washed twice with PBS, and 200 μL of fresh medium plus 10 μL of MTT stock solution (12 mmol/L in PBS) were added to each well. After incubation for 4 h at 37 ˚C and 5% CO_2, 400 μL of DMSO was added to each well and mixed thoroughly before finally measuring the absorbance of the solution at 550 nm.

2.6 Fluorescence imaging of AgNC-stained HeLa cells

HeLa cells were seeded in 8-well LabTek chambers (Nalge Nunc International, New York) and allowed to adhere over night at 37 ˚C and 5% CO_2. After removing the medium by twice washing with PBS, cells were incubated with 25 μg/mL AgNCs in serum-free DMEM with or without 100 μmol/L HSA at 37 ˚C and 5% CO_2 for 2 h. Subsequently, cells were washed three times with PBS. Cell membranes were stained with 0.25 μg/mL of CellMask™ DeepRed in PBS for 5 min and washed twice with PBS. Fluorescence imaging was performed using an Andor Revolution® XD spinning disk laser scanning microscopy system (BFi OPTiLAS, München, Germany). This setup is based on an inverted microscope (Olympus IX81S1F-ZDC, Tokyo, Japan) equipped with an oil immersion objective (APON 60XOTIRF, numerical aperture 1.49, Olympus, Tokyo, Japan), CO_2 and temperature control (5% CO_2 and 37 ˚C, Tokai Hit, Shizuoka-ken, Japan), a CSU-X1 scan head (Yokogawa, Tokyo, Japan) and a DU897 EMCCD camera (Andor, Belfast, UK). AgNC fluorescence was excited at 405 nm; the emission was recorded through a 635 nm long-pass filter (BrightLine 635/LP, AHF, Tübingen, Germany), referred to as the 'green' channel, whereas the emission of the membrane stain CellMask™ DeepRed was detected through a band-pass filter 685/40 (AHF, Tübingen, Germany) upon excitation at 640 nm, referred to as the 'red' channel. Appropriate control experiments ensured that crosstalk between the two channels was negligible.

3. Results and discussion

3.1 Characterization of AgNCs

The formation of AgNCs was evidenced by a gradual color change of the reaction solution from turbid yellow to clear reddish, and bright red emission from the solution could be observed under a UV lamp. The UV–Vis absorption spectrum of DHLA–AgNCs in aqueous solution exhibits three absorption bands centered on 330 nm, 425 nm and 500 nm (Fig. 1(a)), similar as those reported previously [27]. Upon excitation at 425 nm, AgNCs display an intense emission band with a maximum at 630 nm. The QY of these fluorescent AgNCs in PBS was measured to be 2.4% using sulforhodamine 101 (QY = 1.0 in ethanol) as a reference. Unlike larger metal nanoparticles, these few-atom AgNCs cannot support plasmons. Rather, they have molecule-like behavior, exhibiting discrete energy levels, characteristic electronic absorption bands and substantial photoluminescence [30, 31].

A typical AFM image of AgNCs (Fig. 1(b)) shows that the AgNCs are well dispersed on the mica surface. By measuring the maximum height of each particle, an average diameter of AgNCs can be estimated as 1.3 nm ± 0.3 nm. Attempts to measure the core size of AgNCs with high-resolution transmission electron microscopy (HRTEM) led to the observation of larger particles or aggregates, which likely result from the high energy electron-beam irradiation during the TEM measurement [32]. The hydrodynamic diameter of DHLA–AgNCs in PBS was 2.1 nm ± 0.4 nm, determined by DLS (Fig. 1(c)). The extremely small particle size offers a unique advantage of fluorescent AgNCs over other luminescent nanomaterials as optical labels in biological research [33].

XPS measurements were carried out to analyze the valence states of silver and sulfur in DHLA–AgNCs (Fig. 1(d)). The Ag 3d XPS spectrum shows the binding energy (BE) of Ag $3d_{5/2}$ and Ag $3d_{3/2}$ at 368.6 eV and 374.5 eV, respectively, which are close to that of Ag(0) [34], confirming the formation of metallic AgNCs. Moreover, the S 2p signal displays a doublet with the

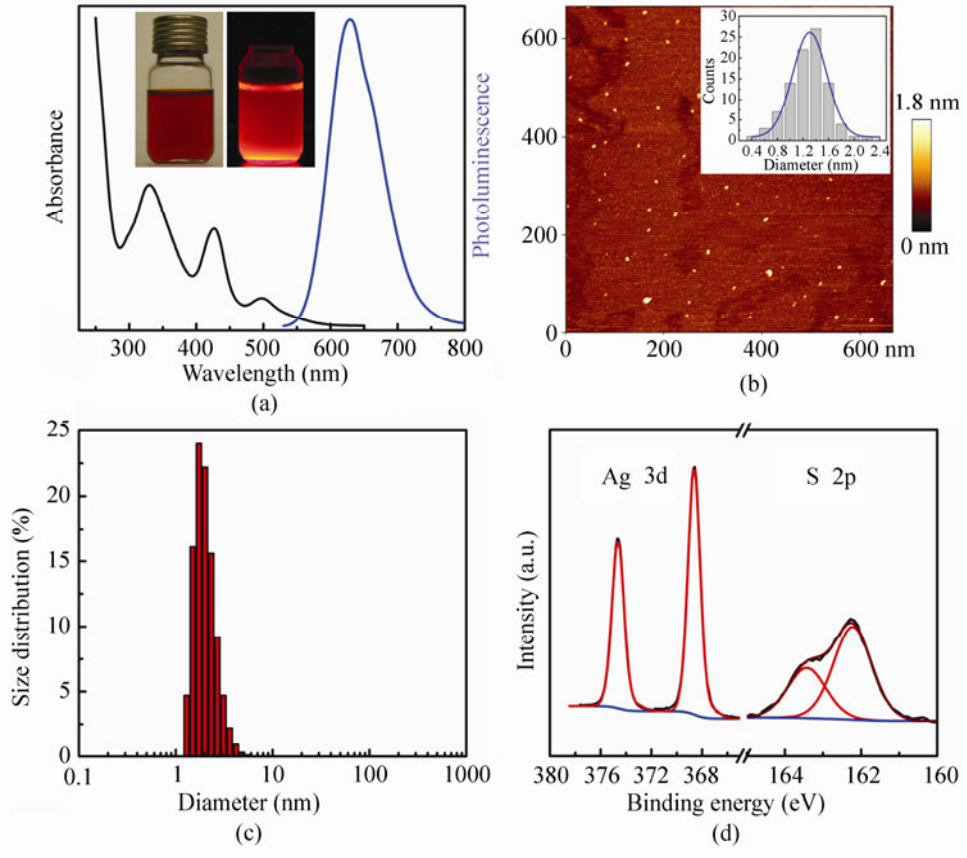

Figure 1 Characterization of DHLA–AgNC properties by different methods. (a) Absorption (black) and fluorescence emission (blue, excitation at 425 nm) spectra of AgNCs in aqueous solution. The inset shows photographs of DHLA–AgNCs (left) in room light and (right) under a UV source emitting 365-nm light. (b) Typical AFM image of AgNCs on a mica surface. The inset shows the size distribution histogram. (c) Size distribution of DHLA–AgNCs in aqueous solution as determined by DLS. (d) Ag 3d and S 2p XPS spectra of AgNCs

S $2p_{3/2}$ peak at a BE of 162.2 eV, which can be assigned to sulfur atoms bound to silver surfaces as thiolate species [35]. Note that the typical band representing oxidized sulfur (at about 168.0 eV) was absent from the S 2p region, in contrast to many previous studies of metal NCs [36–38], indicating a good stability of DHLA-capped AgNCs.

The colloidal stability of DHLA–AgNCs was characterized by measuring their zeta potential in the buffer solution (PBS, pH 7.4), which yielded a value of –51 mV ± 1 mV. Typically, a zeta potential below –30 mV is considered as an indication of a colloidally stable system. Indeed, these clusters were stable for over 2 months without any precipitation. Regarding potential applications of fluorescent AgNCs in cell biology, it is also essential to investigate their stability in cell culture media, e.g., DMEM supplemented with 10% fetal bovine serum [39]. Therefore, absorption spectra of DHLA–AgNCs in the cell medium were monitored for 72 h. As shown in Fig. 2, the absorbance of AgNCs increased slightly during the first 12 h and remained essentially unchanged afterwards. The observed increase of AgNC absorbance in the beginning is likely caused by the adsorption of biomolecules from the cell medium (such as serum proteins) on the particle surface, considering that the optical properties of metal NCs are very sensitive to their surface environment [22]. Taken together, these results demonstrate that DHLA–AgNCs possess a very good stability in the biological medium, which is important for biological applications.

3.2 Interactions of AgNCs with HSA

We investigated the interaction of AgNCs with HSA by using steady-state fluorescence spectroscopy. The fluorescence intensity of AgNCs was observed increases

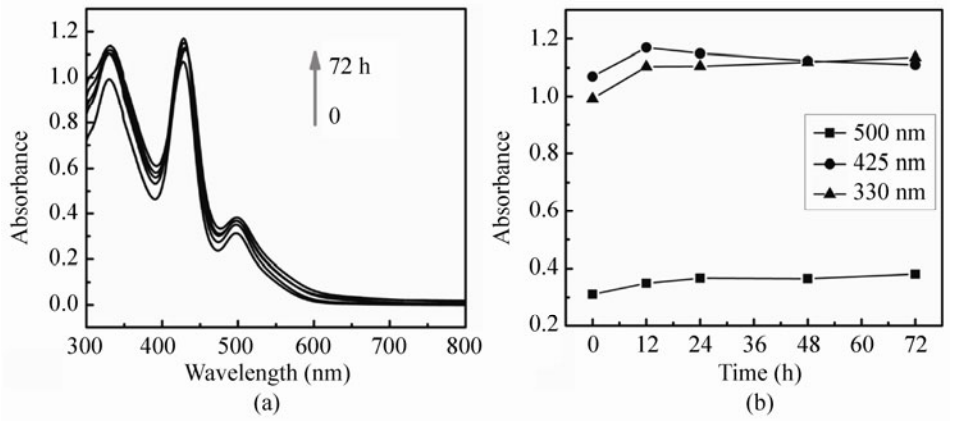

Figure 2 Stability of DHLA–AgNCs in cell medium. (a) Evolution of the absorption spectra in the cell culture medium, DMEM supplemented with 10% fetal bovine serum, within 72 h. (b) Absorbance of DHLA–AgNCs at different wavelengths versus the incubation time

by two-fold when HSA is present in the solution (Fig. 3(a)). Since HSA is non-fluorescent in this spectral range, the luminescence change apparently results from NC–protein interactions. For AuNCs, a luminescence enhancement was also observed as a result of protein adsorption [22]. In addition to the increased fluorescence emission, the fluorescence decay kinetics of AgNCs were also modified (Fig. 3(b)). In the presence of HSA, the fluorescence decay became slower, with the average lifetime increasing from 5.6 ns ± 0.3 ns to 6.8 ns ± 0.4 ns. These results indicate clear changes of the photophysical properties of the AgNCs upon the protein adsorption.

The interactions between proteins and AgNCs also lead to a remarkable change of the intrinsic protein fluorescence. The emission of HSA derives mainly from tryptophan residue 214 (Trp 214), and the fluorescence emission of Trp 214 can be utilized to probe interactions of HSA with nanomaterials [40, 41]. With increasing AgNC concentration, the fluorescence intensity of HSA gradually decreased (Fig.4(a)). Once the protein associates with AgNCs, efficient energy transfer from Trp 214 to AgNCs can take place due to the large overlap between the emission spectrum of HSA and absorption spectrum of AgNCs [42]. As a result, the tryptophan fluorescence is quenched.

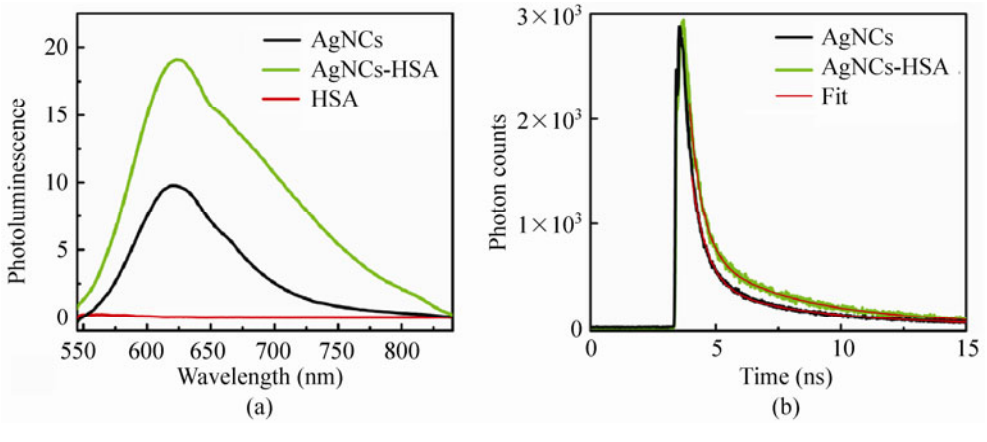

Figure 3 (a) Fluorescence emission spectra of HSA (red) and DHLA–AgNCs (2.8 μmol/L) in the absence (black) and presence of 1.0 μmol/L HSA (green), taken with excitation at 425 nm. (b) Fluorescence decay traces of DHLA–AgNCs (2.8 μmol/L) in the absence (black) and presence of 1.0 μmol/L HSA (green), and the fit curves (red). The emission was collected through a band-pass filter 617/73, upon excitation at 405 nm

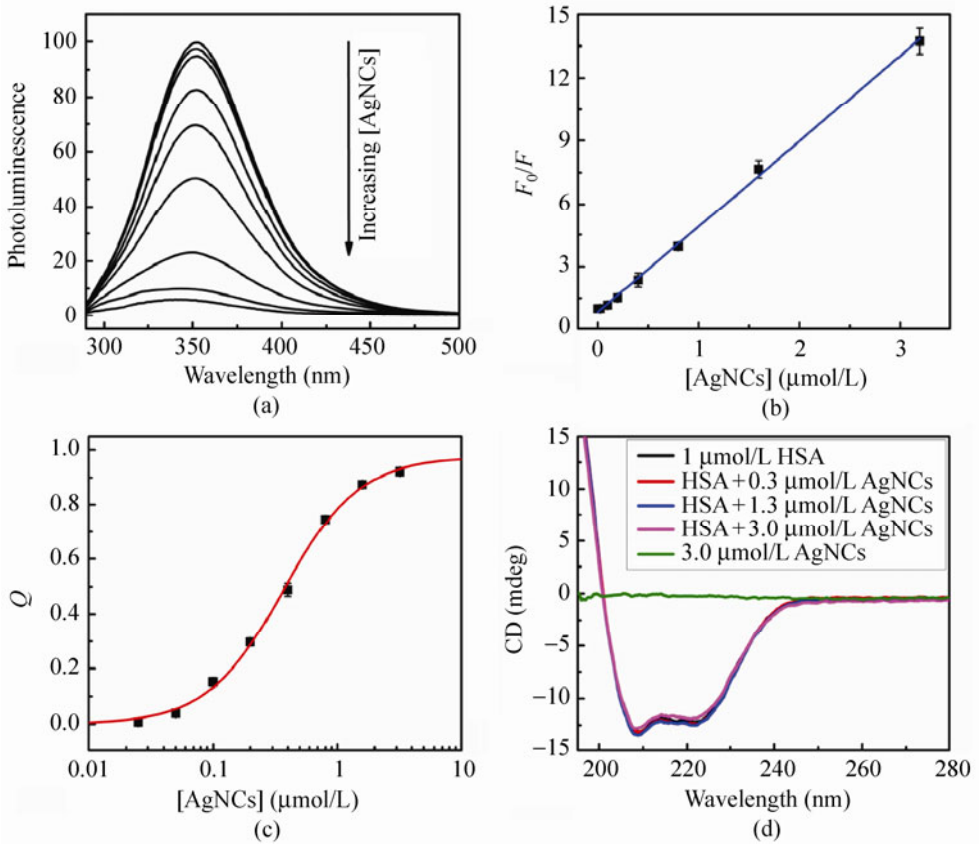

Figure 4 (a) Fluorescence emission spectra of HSA (0.5 μmol/L) upon varying concentration of DHLA–AgNCs (0–3.2μmol/L), taken with excitation at 280 nm. (b) Plots of (F_0/F) as a function of the AgNC concentration. The blue line represents a fit to the data using Eq. 1. (c) Plots of quenching efficiency versus the concentration of AgNCs. The red line represents a fit using Eq. 2. (d) CD spectra of AgNCs and HSA in the presence of different concentrations of AgNCs

The observed fluorescence quenching can be analyzed quantitatively with the Stern–Volmer equation [43],

$$\frac{F_0}{F} = 1 + K_{SV}[\text{AgNCs}] \quad (1)$$

where F_0 and F are the fluorescence intensities in the absence and presence of AgNCs, respectively; K_{SV} is the Stern–Volmer fluorescence quenching constant, which is a measure of the quenching efficiency. Fig. 4(b) shows the Stern–Volmer plots, F_0/F versus [AgNCs] in the concentration range of 0–3.2 μmol/L. By fitting a line to the data according to Eq. 1, we obtained the value of K_{SV}, $(4.1 \pm 0.1) \times 10^6$ mol/L, which is ca. three orders of magnitude lower than that of 60 nm-sized silver nanoparticles [44]. The low quenching efficiency of these ultrasmall AgNCs can be rationalized by the strong size dependence [45, 46]; smaller metal particles quench the emission of adjacent fluorophores less efficiently. The good linearity of plots in the studied concentration range (correlation coefficient $R^2 = 0.999$ from the least squares fit) implies that there is a single dominant mechanism responsible for static quenching due to AgNC–HSA complex formation.

We gained further insight into the binding of AgNCs to HSA by analyzing the fluorescence data by using the Hill equation [22, 47],

$$\frac{Q}{Q_{max}} = \frac{1}{1 + (K_D/[\text{AgNCs}])^n} \quad \text{with} \quad Q = \frac{F_0 - F}{F} \quad (2)$$

where Q_{max} is the saturation value of the quenching efficiency Q; K_D is the midpoint concentration (apparent dissociation coefficient) that quantifies the strength of protein–NC interactions, and n is the Hill coefficient, which controls the steepness of the transition. As

shown in Fig. 4(c), an excellent agreement was achieved by fitting Q/Q_{max} as a function of the AgNC concentration ([AgNCs]) with Eq. 2, yielding K_D = (3.7 ± 0.2) ×10^{-7} mol/L. This value is in the range of K_D values reported for HSA adsorption onto larger metal nanoparticles [47].

The emission spectrum of tryptophan is very sensitive to its local environment in a protein, and its position may shift if the protein changes its conformation. Upon adsorption of HSA onto AgNCs, the emission maximum stayed essentially constant; only a slight blue-shift is visible at high AgNC concentration. This behavior suggests that major perturbations of the protein conformation upon adsorption onto the NC surfaces are absent. Moreover, our CD results confirmed that the characteristic bands of HSA at 208 nm and 222 nm remained essentially unchanged when AgNCs are present in the solution (Fig. 4(d)), suggesting that the secondary structure of HSA is negligibly modified in the NC–protein complex. In contrast, many other studies reported substantial conformational changes of proteins upon surface adsorption onto nanoscale materials [40, 48, 49]. Since the conformation of proteins is intimately related to their biological function, it is of great importance that they retain their native structure within nano–bio conjugates. In this regard, labeling of proteins with nanoprobes that minimally affect their structure, such as the AgNCs shown in the present work, offers distinct advantages in biological research.

3.3 Effect of protein adsorption on the cellular responses of AgNCs

The adsorption of proteins onto AgNCs naturally raises the question as to whether NC–protein interactions affect biological responses of these ultrasmall particles and, in particular, modify the uptake by living cells. Toward this goal, we employed live-cell fluorescence microscopy for facile monitoring the cellular uptake of luminescent nanoparticles with high spatial resolution [50, 51]. Upon incubation of HeLa cells with AgNCs in serum-free DMEM for 2 h, intense fluorescence emission from AgNCs was observed from inside the cells, suggesting an efficient internalization of these luminescent particles by the cells (Fig. 5(c)). Apparently, these ultrasmall AgNCs are taken up

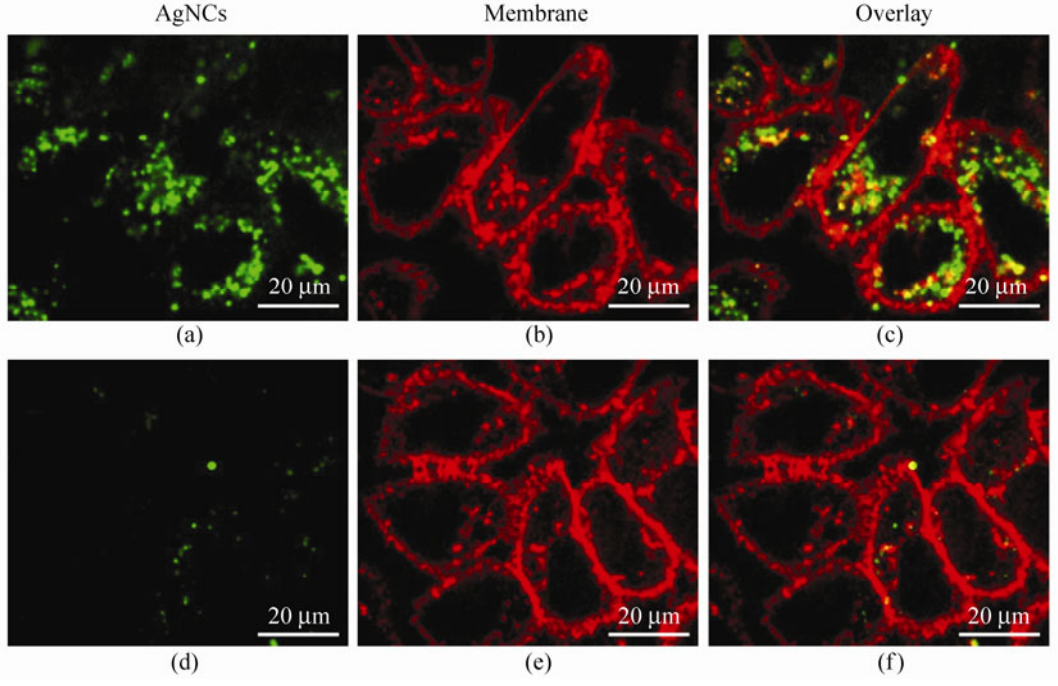

Figure 5 Confocal fluorescence images of HeLa cells upon incubation with DHLA–AgNCs (25 μg/mL) for 2 h in DMEM medium without ((a)–(c)) and with 100 μmol/L HSA ((d)–(f)). Cell membranes were stained with CellMask™ DeepRed ((b) and (e))

by the cell without the aid of additional agents, suggesting their potential utilization as intracellular probes. Nanoparticles internalization can occur via several different endocytosis pathways [52–54]; the detailed mechanisms require further investigation, however.

For studying the effect of protein adsorption on cellular uptake, we performed AgNC uptake experiments in the same medium but with added proteins (100 μmol/L HSA). In contrast to the pronounced uptake of bare AgNCs, the amount of AgNCs internalized by the cells is substantially reduced in the presence of HSA, as seen from the much lower fluorescence intensity (Fig. 5(d)). We analyzed the fluorescence images quantitatively to distinguish particles located in the cell membrane region from those inside the cells (Fig. 6). These results show that the total cellular fluorescence is reduced by approximately eight-fold due to the presence of HSA. While the fluorescence from intracellular AgNCs is stronger than that from membrane-associated particles in both cases, the fluorescence decrease in the membrane region (ca. 13-fold) is much larger than for inside the cells (ca. seven-fold). It is evident that the protein adsorption affects the nanoparticle uptake

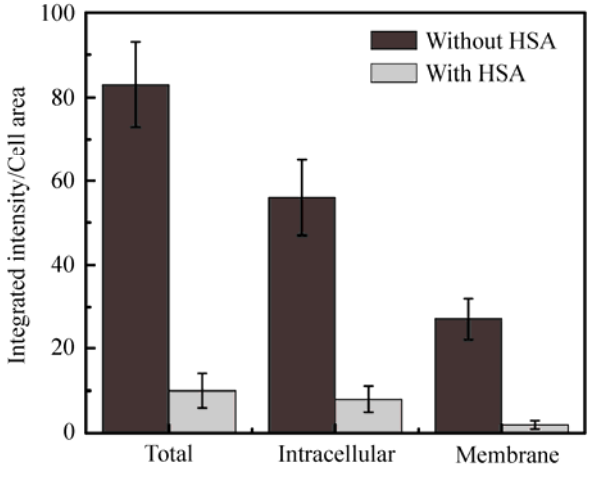

Figure 6 Quantitative analysis of AgNC uptake by HeLa cells upon incubation for 2 h. Total integrated intensity of AgNCs per cell area and separation into intracellular and membrane-associated AgNCs after incubation with 25 μg/mL AgNCs in the absence (dark grey) and presence (light grey) of 100 μmol/L HSA. Results are averages over at least fifty cells

behavior, and the studied protein in the present work, HSA, can suppress the cellular uptake of AgNCs [20]. HSA is known as a kind of "bystander" protein, that is, a protein for which no specific cellular recognition machinery exists [55]. Thus, the adsorbed serum proteins actually act as a protective layer, shielding the NC surface from interactions with the cells. Correspondingly, much fewer AgNCs can be internalized into the cells in comparison to naked particles.

We have carried out further experiments to explore whether the surface coating of proteins influences the cytotoxicity of AgNCs. The viability of HeLa cells, examined by MTT assays, at different AgNC concentrations in the culture medium with and without proteins, can be seen in Fig. 7(a). With increasing AgNC concentration, the cell viability gradually decreased. Over the concentration range examined, one can clearly observe that cell viability in medium with HSA is higher than that in medium without HSA, suggesting a significant role of HSA to the toxicity of AgNCs. To further clarify the effect of protein adsorption on the cytotoxicity of AgNCs, cell viability was measured in the medium with different concentrations of protein (Fig. 7(b)). Evidently, the more proteins are present in the medium, the weaker is the cytotoxic effect of the AgNCs. Previous studies, which revealed that the cytotoxicity of carbon nanoparticles [56], metal oxide nanoparticles [57] and carbon nanotubes [58] could be reduced by the adsorption of serum proteins, agree well with our present findings. Although a comprehensive understanding of the toxic mechanism of AgNCs has remained elusive as yet, a possible and most sensible reason for the reduced cytotoxicity of AgNCs is that the presence of HSA in the medium significantly reduces the amount of AgNCs internalized by the cells, as shown by our fluorescence microscopy results. Moreover, proteins on the particle surfaces may possibly shield the inherent toxicity of AgNCs. While the detailed mechanisms of intrinsic toxicity of AgNCs and its protein dependence call for further studies, we can conclude that protein adsorption has a significant influence on cellular responses of AgNCs.

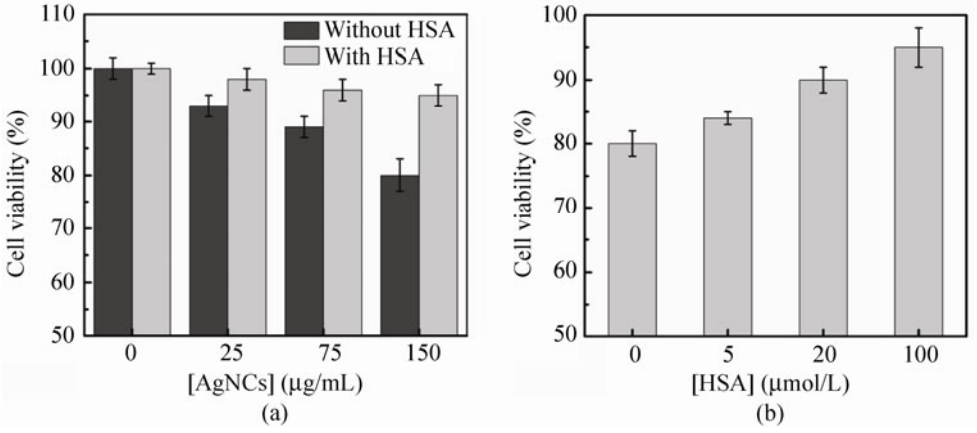

Figure 7 Effect of protein adsorption on the cytotoxicity of AgNCs. (a) Viability of HeLa cells after 24 h of incubation with different concentrations of AgNCs in the cell medium without (dark grey) and with 100 μmol/L HSA (light grey), as determined by MTT assays. (b) Viability of HeLa cells after 24 h of incubation with 150 μg/mL AgNCs in the cell medium with different concentrations of HSA. The error bars represent variations among four independent measurements

4. Conclusions

We have studied the interaction of ultrasmall fluorescent AgNCs with proteins and explored the resulting biological consequences. Taking HSA as a model protein, we demonstrated that protein adsorption can have a substantial effect on the physicochemical properties of both AgNCs and proteins; particularly, the photophysical properties of AgNCs are significantly modified. Moreover, the effects of protein adsorption on the biological responses of AgNCs were quantitatively evaluated by fluorescence microscopy and cytotoxicity experiments, which gave clear evidence that protein adsorption markedly changes the uptake behavior as well the cytotoxicity of AgNCs. These results and future work on exploring the behavior of AgNCs in more complex biological environment will be valuable for designing optimal AgNC-based materials and advancing their application in the areas such as biosensing, drug delivery and cell diagnosis. Furthermore, considering the great concerns voiced about nanoparticle toxicity in recent years, the present findings provide a further understanding of nanomaterials, especially metal NCs, which will be helpful in designing and utilizing them for safe biomedical applications.

Acknowledgements

G.U.N. was supported by the Deutsche Forschungsgemeinschaft (DFG) through the Center for Functional Nanostructures (CFN) and the Priority Program SPP1313. L. S. gratefully acknowledges support from the Alexander von Humboldt (AvH) Foundation. The authors would like to thank Mr. Christoph Panther and Dr. Clemens Franz for help with the AFM measurements.

References

[1] Cao, Y. C. Nanomaterials for biomedical applications. *Nanomedicine* **2008**, *3*, 467–469.

[2] Zhang, J. J.; Du, J. J.; Yan, M.; Dhaliwal, A.; Wen, J.; Liu, F. Q.; Segura, T.; Lu, Y. F. Synthesis of protein nanoconjugates for cancer therapy. *Nano Res.* **2011**, *4*, 425–433.

[3] Chi, X. Q.; Huang, D. T.; Zhao, Z. H.; Zhou, Z. J.; Yin, Z. Y.; Gao, J. H. Nanoprobes for in vitro diagnostics of cancer and infectious diseases. *Biomaterials* **2012**, *33*, 189–206.

[4] Shang, L.; Dong, S. J.; Nienhaus, G. U. Ultra-small fluorescent metal nanoclusters: Synthesis and biological applications. *Nano Today* **2011**, *6*, 401–418.

[5] Zheng, J.; Nicovich, P. R.; Dickson, R. M. Highly fluorescent noble-metal quantum dots. *Ann. Rev. Phys. Chem.* **2007**, *58*, 409–431.

[6] Sharma, J.; Yeh, H. C.; Yoo, H.; Werner, J. H.; Martinez, J. S. A complementary palette of fluorescent silver nanoclusters. *Chem. Commun.* **2010**, *46*, 3280–3282.

[7] Patel, S. A.; Richards, C. I.; Hsiang, J. C.; Dickson, R. M. Water-soluble Ag nanoclusters exhibit strong two-photon-induced fluorescence. *J. Am. Chem. Soc.* **2008**, *130*, 11602–11603.

[8] Richards, C. I.; Choi, S.; Hsiang, J. C.; Antoku, Y.; Vosch, T.; Bongiorno, A.; Tzeng, Y. L.; Dickson, R. M. Oligonucleotide-stabilized Ag nanocluster fluorophores. *J. Am. Chem. Soc.* **2008**, *130*, 5038–5039.

[9] Yuan, X.; Luo, Z. T.; Zhang, Q. B.; Zhang, X. H.; Zheng, Y. G.; Lee, J. Y.; Xie, J. P. Synthesis of highly fluorescent metal (Ag, Au, Pt, and Cu) nanoclusters by electrostatically induced reversible phase transfer. *ACS Nano* **2011**, *5*, 8800–8808.

[10] Yu, J. H.; Choi, S. M.; Richards, C. I.; Antoku, Y.; Dickson, R. M. Live cell surface labeling with fluorescent Ag nanocluster conjugates. *Photochem. Photobiol.* **2008**, *84*, 1435–1439.

[11] Diez, I.; Ras, R. H. A. Fluorescent silver nanoclusters. *Nanoscale* **2011**, *3*, 1963–1970.

[12] Choi, S.; Dickson, R. M.; Yu, J. H. Developing luminescent silver nanodots for biological applications. *Chem. Soc. Rev.* **2012**, *41*, 1867–1891.

[13] Huang, S.; Pfeiffer, C.; Hollmann, J.; Friede, S.; Chen, J. J. C.; Beyer, A.; Haas, B.; Volz, K.; Heimbrodt, W.; Montenegro Martos, J. M., et al. Synthesis and characterization of colloidal fluorescent silver nanoclusters. *Langmuir* **2012**, *28*, 8915–8919.

[14] Guo, W. W.; Yuan, J. P.; Dong, Q. Z.; Wang, E. K. Highly sequence-dependent formation of fluorescent silver nanoclusters in hybridized DNA duplexes for single nucleotide mutation identification. *J. Am. Chem. Soc.* **2010**, *132*, 932–934.

[15] Yu, J.; Patel, S. A.; Dickson, R. M. In vitro and intracellular production of peptide-encapsulated fluorescent silver nanoclusters. *Angew. Chem. Int. Ed.* **2007**, *46*, 2028–2030.

[16] Yin, J. J.; He, X. X.; Wang, K. M.; Qing, Z. H.; Wu, X.; Shi, H.; Yang, X. H. One-step engineering of silver nanoclusters–aptamer assemblies as luminescent labels to target tumor cells. *Nanoscale* **2012**, *4*, 110–112.

[17] Cedervall, T.; Lynch, I.; Lindman, S.; Berggård, T.; Thulin, E.; Nilsson, H.; Dawson, K. A.; Linse, S. Understanding the nanoparticle–protein corona using methods to quantify exchange rates and affinities of proteins for nanoparticles. *Proc. Natl. Acad. Sci. U. S. A.* **2007**, *104*, 2050–2055.

[18] Nel, A. E.; Madler, L.; Velegol, D.; Xia, T.; Hoek, E. M. V.; Somasundaran, P.; Klaessig, F.; Castranova, V.; Thompson, M. Understanding biophysicochemical interactions at the nano–bio interface. *Nat. Mater.* **2009**, *8*, 543–557.

[19] Röcker, C.; Pötzl, M.; Zhang, F.; Parak, W. J.; Nienhaus, G. U. A quantitative fluorescence study of protein monolayer formation on colloidal nanoparticles. *Nat. Nanotechnol.* **2009**, *4*, 577–580.

[20] Jiang, X.; Weise, S.; Hafner, M.; Röcker, C.; Zhang, F.; Parak, W. J.; Nienhaus, G. U. Quantitative analysis of the protein corona on FePt nanoparticles formed by transferrin binding. *J. R. Soc. Interface* **2010**, *7*, S5–S13.

[21] Treuel, L.; Nienhaus, G. U. Toward a molecular understanding of nanoparticle–protein interactions. *Biophys. Rev.* **2012**, *4*, 137–147.

[22] Shang, L.; Brandholt, S.; Stockmar, F.; Trouillet, V.; Bruns, M.; Nienhaus, G. U. Effect of protein adsorption on the fluorescence of ultrasmall gold nanoclusters. *Small* **2012**, *8*, 661–665.

[23] Lundqvist, M.; Stigler, J.; Elia, G.; Lynch, I.; Cedervall, T.; Dawson, K. A. Nanoparticle size and surface properties determine the protein corona with possible implications for biological impacts. *Proc. Natl. Acad. Sci. U. S. A.* **2008**, *105*, 14265–14270.

[24] Shang, L.; Nienhaus, G. U. Gold nanoclusters as novel optical probes for in vitro and *in vivo* fluorescence imaging. *Biophys. Rev.* **2012**, DOI: 10.1007/s12551-012-0076-9.

[25] Xie, J.; Zheng, Y. G.; Ying, J. Y. Protein-directed synthesis of highly fluorescent gold nanoclusters. *J. Am. Chem. Soc.* **2009**, *131*, 888–889.

[26] Xavier, P. L.; Chaudhari, K.; Baksi, A.; Pradeep, T. Protein-protected luminescent noble metal quantum clusters: An emerging trend in atomic cluster nanoscience. *Nano Rev.* **2012**, *3*, 14767.

[27] Adhikari, B.; Banerjee, A. Facile synthesis of water-soluble fluorescent silver nanoclusters and Hg^{II} sensing. *Chem. Mater.* **2010**, *22*, 4364–4371.

[28] Vinelli, A.; Primiceri, E.; Brucale, M.; Zuccheri, G.; Rinaldi, R.; Samorì, B. Sample preparation for the quick sizing of metal nanoparticles by atomic force microscopy. *Microsc. Res. Techniq.* **2008**, *71*, 870–879.

[29] Shang, L.; Azadfar, N.; Stockmar, F.; Send, W.; Trouillet, V.; Bruns, M.; Gerthsen, D.; Nienhaus, G. U. One-pot synthesis of near-infrared fluorescent gold clusters for cellular fluorescence lifetime imaging. *Small* **2011**, *7*, 2614–2620.

[30] Petty, J. T.; Zheng, J.; Hud, N. V.; Dickson, R. M. DNA-templated Ag nanocluster formation. *J. Am. Chem. Soc.* **2004**, *126*, 5207–5212.

[31] Cathcart, N.; Kitaev, V. Silver nanoclusters: single-stage scaleable synthesis of monodisperse species and their chirooptical properties. *J. Phys. Chem. C* **2010**, *114*, 16010–16017.

[32] Buffat, P. A. Dynamical behaviour of nanocrystals in transmission electron microscopy: Size, temperature or irradiation effects. *Philos. T. Roy. Soc. A* **2003**, *361*, 291–295.

[33] Baker, M. Nanotechnology imaging probes: Smaller and more stable. *Nat. Methods* **2010**, *7*, 957–962.

[34] Zhao, S. Q.; Zhou, Y. L.; Zhao, K.; Liu, Z.; Han, P.; Wang, S. F.; Xiang, W. F.; Chen, Z. H.; Lü, H. B.; Cheng, B. L., et al. Violet luminescence emitted from Ag-nanocluster doped ZnO thin films grown on fused quartz substrates by pulsed laser deposition. *Physica B* **2006**, *373*, 154–156.

[35] Kummer, K.; Vyalikh, D. V.; Gavrila, G.; Kade, A.; Weigel-Jech, M.; Mertig, M.; Molodtsov, S. L. High-resolution photoelectron spectroscopy of self-assembled mercaptohexanol monolayers on gold surfaces. *J. Electron Spectrosc. Relat. Phenom.* **2008**, *163*, 59–64.

[36] Xavier, P. L.; Chaudhari, K.; Verma, P. K.; Pal, S. K.; Pradeep, T. Luminescent quantum clusters of gold in transferrin family protein, lactoferrin exhibiting FRET. *Nanoscale* **2010**, *2*, 2769–2776.

[37] Tang, Z. H.; Xu, B.; Wu, B. H.; Germann, M. W.; Wang, G. L. Synthesis and structural determination of multidentate 2,3-dithiol-stabilized Au clusters. *J. Am. Chem. Soc.* **2010**, *132*, 3367–3374.

[38] Le Guével, X.; Hötzer, B.; Jung, G.; Hollemeyer, K.; Trouillet, V.; Schneider, M. Formation of fluorescent metal (Au, Ag) nanoclusters capped in bovine serum albumin followed by fluorescence and spectroscopy. *J. Phys. Chem. C* **2011**, *115*, 10955–10963.

[39] Nallathamby, P. D.; Xu, X. H. N. Study of cytotoxic and therapeutic effects of stable and purified silver nanoparticles on tumor cells. *Nanoscale* **2010**, *2*, 942–952.

[40] Shang, L.; Wang, Y. Z.; Jiang, J. G.; Dong, S. J. pH-dependent protein conformational changes in albumin:gold nanoparticle bioconjugates: A spectroscopic study. *Langmuir* **2007**, *23*, 2714–2721.

[41] Xiao, Q.; Huang, S.; Qi, Z. D.; Zhou, B.; He, Z. K.; Liu, Y. Conformation, thermodynamics and stoichiometry of HSA adsorbed to colloidal CdSe/ZnS quantum dots. *BBA–Proteins Proteom.* **2008**, *1784*, 1020–1027.

[42] Malta, O. L. Energy transfer between molecules and small metallic particles. *Phys. Lett. A* **1986**, *114*, 195–197.

[43] Lakowicz, J. R. *Principles of Fluorescence Spectroscopy*. 3rd ed.; Springer: New York, 2006.

[44] Mariam, J.; Dongre, P. M.; Kothari, D. C. Study of interaction of silver nanoparticles with bovine serum albumin using fluorescence spectroscopy. *J. Fluoresc.* **2011**, *21*, 2193–2199.

[45] Fan, C. H.; Wang, S.; Hong, J. W.; Bazan, G. C.; Plaxco, K. W.; Heeger, A. J. Beyond superquenching: hyper-efficient energy transfer from conjugated polymers to gold nanoparticles. *Proc. Natl. Acad. Sci. U S A* **2003**, *100*, 6297–6301.

[46] Ghosh, S. K.; Pal, A.; Kundu, S.; Nath, S.; Pal, T. Fluorescence quenching of 1-methylaminopyrene near gold nanoparticles: size regime dependence of the small metallic particles. *Chem. Phys. Lett.* **2004**, *395*, 366–372.

[47] Lacerda, S. H. D.; Park, J. J.; Meuse, C.; Pristinski, D.; Becker, M. L.; Karim, A.; Douglas, J. F. Interaction of gold nanoparticles with common human blood proteins. *ACS Nano* **2009**, *4*, 365–379.

[48] Zhang, D. M.; Neumann, O.; Wang, H.; Yuwono, V. M.; Barhoumi, A.; Perham, M.; Hartgerink, J. D.; Wittung-Stafshede, P.; Halas, N. J. Gold nanoparticles can induce the formation of protein-based aggregates at physiological pH. *Nano Lett.* **2009**, *9*, 666–671.

[49] Wang, J.; Jensen, U. B.; Jensen, G. V.; Shipovskov, S.; Balakrishnan, V. S.; Otzen, D.; Pedersen, J. S.; Besenbacher, F.; Sutherland, D. S. Soft interactions at nanoparticles alter protein function and conformation in a size dependent manner. *Nano Lett.* **2011**, *11*, 4985–4991.

[50] Ohulchanskyy, T. Y.; Roy, I.; Yong, K. T.; Pudavar, H. E.; Prasad, P. N. High-resolution light microscopy using luminescent nanoparticles. *Wiley Interdiscip. Rev. Nanomed. Nanobiotechnol.* **2010**, *2*, 162–175.

[51] Hedde, P. N.; Nienhaus, G. U. Optical imaging of nanoscale cellular structures. *Biophys. Rev.* **2010**, *2*, 147–158.

[52] Jiang, X. E.; Röcker, C.; Hafner, M.; Brandholt, S.; Dörlich, R. M.; Nienhaus, G. U. Endo- and exocytosis of zwitterionic quantum dot nanoparticles by live HeLa cells. *ACS Nano* **2010**, *4*, 6787–6797.

[53] Lunov, O.; Zablotskii, V.; Syrovets, T.; Röcker, C.; Tron, K.; Nienhaus, G. U.; Simmet, T. Modeling receptor-mediated endocytosis of polymer-functionalized iron oxide nanoparticles by human macrophages. *Biomaterials* **2011**, *32*, 547–555.

[54] Iversen, T. G.; Skotland, T.; Sandvig, K. Endocytosis and intracellular transport of nanoparticles: Present knowledge and need for future studies. *Nano Today* **2011**, *6*, 176–185.

[55] Walczyk, D.; Bombelli, F. B.; Monopoli, M. P.; Lynch, I.; Dawson, K. A. What the cell "sees" in bionanoscience. *J. Am. Chem. Soc.* **2010**, *132*, 5761–5768.

[56] Zhu, Y.; Li, W. X.; Li, Q. N.; Li, Y. G.; Li, Y. F.; Zhang, X. Y.; Huang, Q. Effects of serum proteins on intracellular uptake and cytotoxicity of carbon nanoparticles. *Carbon* **2009**, *47*, 1351–1358.

[57] Horie, M.; Nishio, K.; Fujita, K.; Endoh, S.; Miyauchi, A.; Saito, Y.; Iwahashi, H.; Yamamoto, K.; Murayama, H.; Nakano, H., et al. Protein adsorption of ultrafine metal oxide and its influence on cytotoxicity toward cultured cells. *Chem. Res. Toxicol.* **2009**, *22*, 543–553.

[58] Ge, C. C.; Du, J. F.; Zhao, L. N.; Wang, L. M.; Liu, Y.; Li, D. H.; Yang, Y. L.; Zhou, R. H.; Zhao, Y. L.; Chai, Z. F., et al. Binding of blood proteins to carbon nanotubes reduces cytotoxicity. *Proc. Natl. Acad. Sci. U S A* **2011**, *108*, 16968–16973.